Preprint Title Design of a Wearable Flexible Nano-Heart Sound Sensor Based on P(VDF-TrFE)/ZnO/GR and Its Application in Cardiac Disease Detection

Authors Yi Luo, Jian Liu, Jiachang Zhang, Yu Xiao, Ying Wu and Zhidong Zhao

Publication Date 30 Mai 2023

Article Type Full Research Paper

ORCID® iDs Yi Luo - https://orcid.org/0009-0007-4797-4098; Jian Liu - https://orcid.org/0009-0007-6816-3948; Jiachang Zhang - https://orcid.org/0000-0002-6636-0135; Yu Xiao - https://orcid.org/0009-0007-7909-6410; Ying Wu - https://orcid.org/0009-0003-2722-731X; Zhidong Zhao - https://orcid.org/0009-0008-7945-8466

Design of a Wearable Flexible Nano-Heart Sound Sensor Based on P(VDF-TrFE)/ZnO/GR and Its Application in Cardiac Disease Detection

Yi Luo[1], Jian Liu[2], Jiachang Zhang[1], Yu Xiao[2], Ying Wu[3] and Zhidong Zhao[4]*

Address:

[1]School of Electronics and Information Engineering, Hangzhou DIANZI University, Hangzhou 310018, China

[2]School of Communication Engineering, Hangzhou DIANZI University, Hangzhou 310018, China

[3]Academic Affairs Office, Hangzhou DIANZI University, Hangzhou 310018, China

[4]School of Cyberspace Security, Hangzhou DIANZI University, Hangzhou 310018, China

Email: zhaozd@hdu.edu.cn

* Corresponding author

Abstract

This paper proposes a method for preparing flexible composite piezoelectric nanofilms of P(VDF-TrFE)/ZnO/Graphene (GR) using the high-pressure electrospinning method. The composition and β-phase content of the piezoelectric composite films were analyzed using X-ray diffraction (XRD) patterns. The morphology of the composite film fibers was observed through scanning electron microscope (SEM) images. Finally, the P(VDF-TrFE)/ZnO/GR

piezoelectric composite film was encapsulated in a sandwich structure heart sound sensor, and a visual heart sound acquisition and classification system was designed using LabVIEW. A heart sound classification model was trained based on the fine K-Nearest-Neighbor (KNN) classification algorithm to predict whether the collected heart sounds are normal or abnormal. The heart sound detection system designed in this paper can collect heart sound signals in real-time and predict whether the heart sounds are normal or abnormal, providing a new solution for the diagnosis of heart disease.

Keywords

composite piezoelectric nanofilm; heart sound sensor; heart sound stethoscope; electrospinning; Heart sound classification algorithm

Introduction

According to data released by the World Health Organization (WHO), approximately 17.9 million people die each year from cardiovascular disease (CVD) [1]. CVD has always been one of the primary diseases affecting human health. In recent years, the number of cardiovascular patients has continued to increase. Heart sounds are physiological signals generated by the movement of various heart valves, myocardium, blood, and other parts of the heart, which contain a significant amount of pathological information about the heart and blood vessels [2]. Therefore, heart sound auscultation is considered one of the most effective methods for diagnosing CVD.

Auscultation of heart sounds usually requires the aid of a stethoscope. In 1816, the French physician Laennec invented the stethoscope, which was gradually improved to form the

current acoustic stethoscope [3]. The traditional acoustic stethoscope is mainly composed of three parts: the auscultation head, sound guide hose, and ear-hook. It uses the principle of physical sound transmission to collect and transmit the heart sound. In order to overcome the shortcomings of the acoustic stethoscope, which lacks amplification during auscultation, is susceptible to noise, and relies heavily on the practitioner's experience, new stethoscope technologies have emerged as contemporary research hotspots, including electronic stethoscopes [4-5], Doppler stethoscopes [6-7], and Bluetooth heart sound stethoscopes [8]. Piezoelectric materials, which can convert mechanical vibration signals into voltage signals, have become one of the primary materials for creating heart sound sensors [9].

Piezoelectric materials are essential components in heart sound auscultation equipment. When piezoelectric materials are subjected to pressure, they generate a voltage at both ends, thereby converting mechanical energy into electrical energy, a phenomenon known as the positive piezoelectric effect. Most electronic stethoscopes in the market today utilize the positive piezoelectric properties of rigid piezoelectric materials like lead zirconate titanate (Pb(Zr1-xTix)O3, PZT). These materials convert sound wave vibrations into electrical signals that are proportional and then transmitted to the conditioning circuit. After a series of processing steps, the heart sound signal is obtained. However, PZT has a brittle texture, does not fit the skin well, and lacks comfort when worn, making it unsuitable for wearable sensors [10]. Moreover, the lead contained in PZT is harmful to humans. P(VDF-TrFE) is a polymer piezoelectric material with a wide frequency bandwidth, good biocompatibility, and softness. It is one of the preferred materials for flexible piezoelectric sensors [11]. However, compared to rigid piezoelectric materials such as PZT, pure P(VDF-TrFE) has inferior piezoelectric

properties [12]. Researchers have improved the film-making process by adding fillers to P(VDF-TrFE), using secondary polarization, and other methods to enhance its piezoelectric performance. Kumar et al. prepared P(VDF-TrFE)/ZnO matrix composite nanogenerators using electrospinning. The voltage and current of these nanogenerators were 2.4 times and 1.6 times greater than those of pure P(VDF-TrFE) nanogenerators, respectively [13]. Subash et al. added ZnO nanoparticles and peeled graphene oxide (EGO) to P(VDF-TrFE) to prepare a composite nanofilm with excellent touch sensitivity and high output energy. They also used the piezoelectric film for triboelectric piezoelectric energy harvesting [14].

Machine learning is currently a popular topic in the application of classifying heart sound signals and diagnosing heart diseases. The process of analyzing heart sounds mainly involves three parts: signal preprocessing, feature extraction, and classification recognition. The classification methods of heart sound signals can be divided into several types: BP neural network, support vector machine (SVM), Gaussian mixture model (GMM), wavelet neural network, hidden Markov model-based, clustering-based method, etc. For example, Zheng et al. successfully implemented computer-aided diagnosis of chronic heart failure using least squares SVM [15].

To enable real-time monitoring and earlier detection of cardiovascular diseases, a flexible piezoelectric thin film heart sound sensor was developed, and a heart sound detection and classification system was built based on this sensor. In this paper, Zinc oxide (ZnO) and Graphene (GR) fillers were added to the P(VDF-TrFE) matrix, and P(VDF-TrFE)/ZnO/GR composite piezoelectric nanofilms were prepared use a high-pressure electrospinning process. The resulting piezoelectric nanofilm was encapsulated into a wearable, flexible heart

sound sensor for detecting heart sounds. A heart sound detection system was then built using LabVIEW software, which detects heart sounds and extracts features from the preprocessed heart sound signals using MATLAB scripts. Finally, a K-Nearest-Neighbor (KNN) heart sound classification model was trained and used to predict whether a heart sound is normal or abnormal, with the prediction result displayed.

Experimental

Preparation of Films by High-voltage Electrospinning

In this paper, composite piezoelectric nanofilms were prepared using a high-voltage electrospinning process. This process comprises of three main components: a high-voltage DC power supply, micro-pump spinnerets, and a fiber collector [16]. The piezoelectric nano-films produced using this process possess flexibility and do not require secondary polarization. Additionally, this technique is cost-effective, convenient, and straightforward, making it an optimal method for preparing piezoelectric nano-films. The specific methodology used to prepare the piezoelectric nanofilms is illustrated in Figure 1. First, P(VDF-TrFE) powder (Solvay in France, molar ratio 7:3) was mixed with N, N-dimethylamide (DMF, Belgian Acros company) and acetone (Sinopharm Chemical Reagent Co., Ltd., evaporation residue) in a mixed solution with a 3:2 volume ratio (<0.001%). The mass fraction of P(VDF-TrFE) was 12%. Second, the reagent bottle was sealed and placed in a shaking mixer and shaken for 3 hours. Next, nano ZnO particles (Shanghai Keyan Industrial Co., Ltd., particle size 3±5nm, content ≥99.8%) and GR filler (Shenzhen Turing Evolution Technology Co., Ltd., carbon content 98%, diameter thickness ratio average 9500) were added to the mixed solution. The

mass fraction of ZnO was 10%, the mass fraction of GR was 0.1%, and then the packing particles in the solution were dispersed by ultrasonic treatment for 2 hours. Finally, the solution was shaken and mixed for 3 hours to obtain the electrospinning solution. The electrospinning solution was aspirated using a 15 mL syringe, placed on a micropump propeller, and propelled at a speed of 1.5 mL/h for high-pressure electrospinning. The voltage was set to 20 kV, and the distance from the needle to the roller collector was set to 13 cm. The ambient temperature and humidity during high-pressure electrospinning were controlled at 25 °C and 40% RH, respectively.

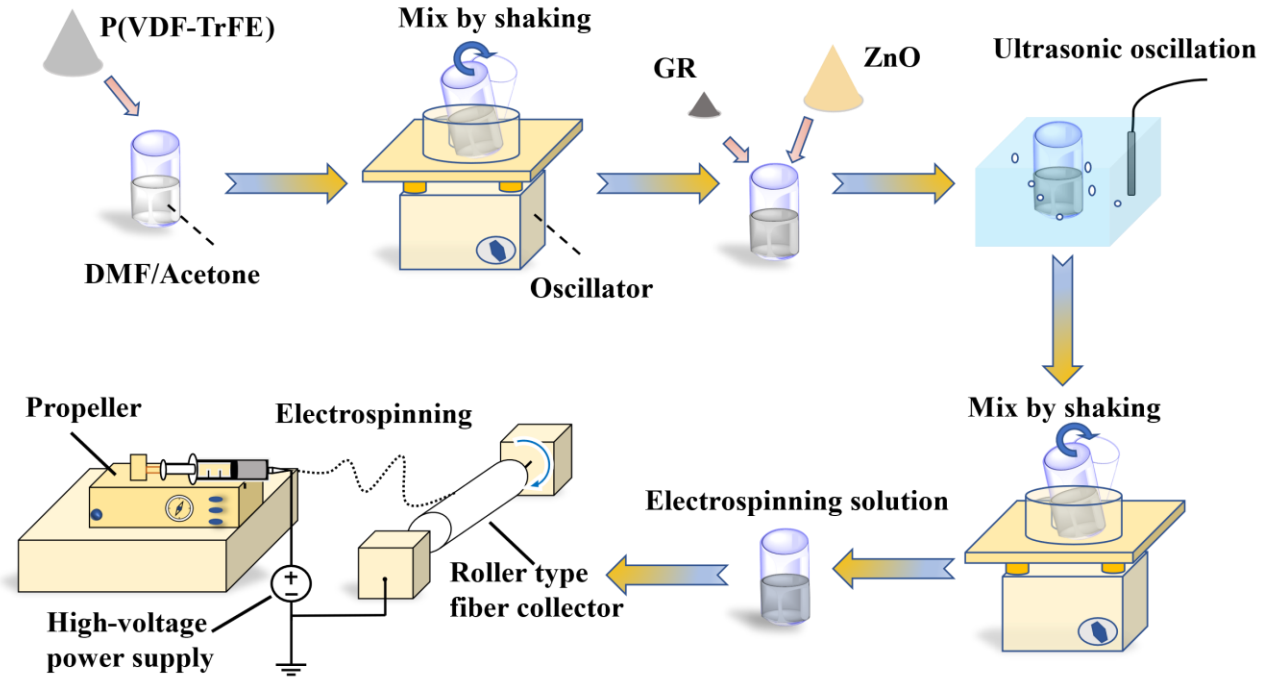

Figure 1: Preparation process of composite nano piezoelectric film

Fabrication of Wearable Flexible Nano Heart Sound Sensors

Figure 2 illustrates the process of creating a wearable, flexible nano-heart sound sensor, which follows a typical sandwich structure. Firstly, a rectangular composite nano-film measuring 4.5 cm in length and 3 cm in width is cut, and a layer of conductive silver paste is

evenly applied to both sides of the film. The paste is then dried completely by heating it on a plate at 55°C for 2 hours. Copper foil tape is used as an electrode to attach to the conductive silver paste layer on both sides, and wires are welded onto the edges of the copper foil to draw out the charge. In the mold shown in the figure, a thin layer of silica gel is injected and left to stand until it is dry. The nano-film attached to the electrode is then placed in the mold, and an appropriate amount of silica gel is slowly injected until the film is completely immersed. After standing for two days, the flexible nano-heart sound sensor is ready for use. Figure 3 displays the actual sensor produced, with Figures 3(a) and 3(b) being photos of the front and back sides of the sensor, and Figures 3(c) and 3(d) being photos of the sensor after bending. It was observed that the sensor encapsulated by silica gel was highly flexible and could fit snugly onto the skin. Additionally, the food-grade silica gel used in the outermost layer is green, harmless to human health, and makes for a great wearable, flexible nano-sensor.

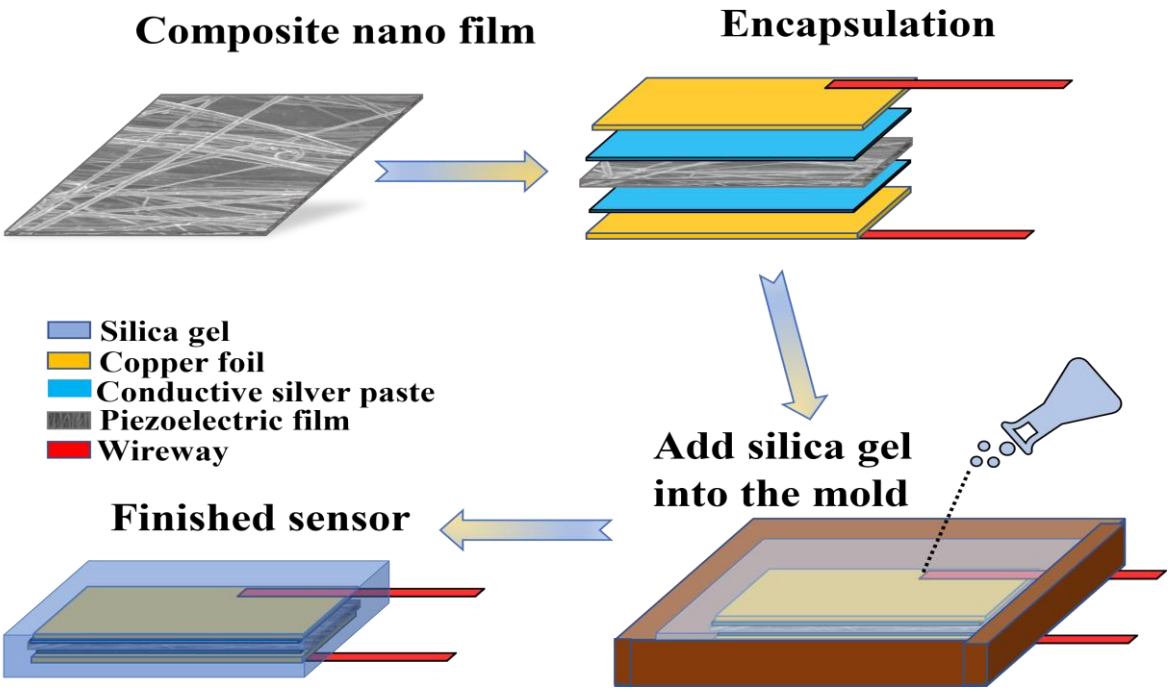

Figure 2: Flexible sensor packaging flow

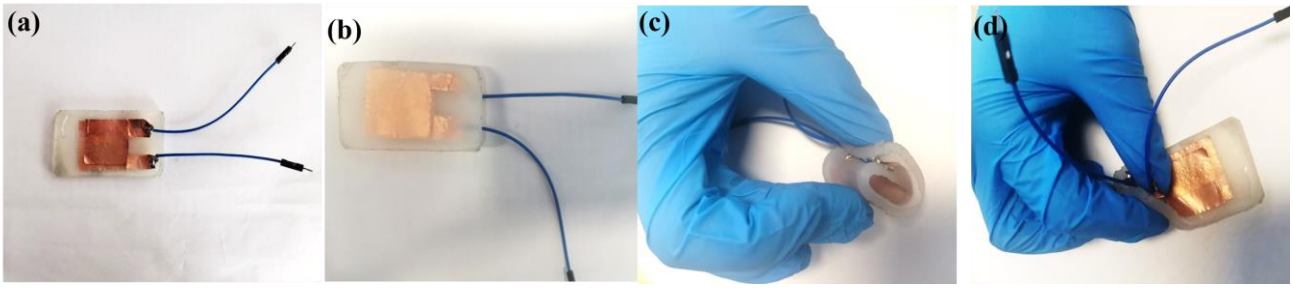

Figure 3: Actual sensor diagram

Construction of Acoustic-electrical Conversion Performance Test Platform

The heart sound sensor needs to convert the sound signal of the heart sound into an electrical signal, requiring the sensor to meet certain requirements in terms of its acoustic and electrical conversion performance. This paper utilized a self-built platform (shown in Figure 4) to evaluate the acoustic-electrical conversion capability of the sensor. The platform consists of an oscilloscope, a charge amplifier, a signal generator, a power amplifier, a speaker, a fixed bracket, and a decibel tester. The signal generator produces a continuous periodic electrical signal, which is then amplified by the power amplifier and delivered to the speaker to convert the electrical signal into an acoustic signal. A flexible nano heart sound sensor is placed 1 cm above the speaker, and its electrodes are connected to the charge amplifier and then to the oscilloscope. The voltage amplitude and frequency displayed on the oscilloscope demonstrate the self-made heart sound sensor's acoustic-electrical conversion ability. The loudspeaker's emitted sound frequency is controlled by setting the signal generator to produce a sine wave signal with different frequencies, while the decibel level of the sound emitted is adjusted by regulating the amplitude of the signal generated and the power amplifier's amplification. During the electroacoustic conversion performance test, a decibel

tester is placed 1.5 cm above the heart sound sensor to control the sound pressure.

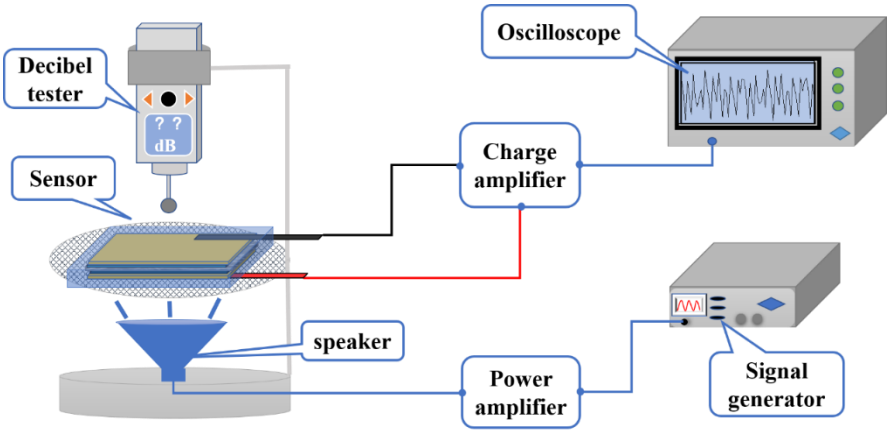

Figure 4: Acoustic-electrical conversion performance test platform

Construction of Heart Sound Acquisition and Classification System

The experiment involved setting up a heart sound acquisition and classification system as illustrated in Figure 5. The experimental flexible nano-heart sound sensor was connected to a charge amplifier with a charge amplification set to 100pC/V. The open-circuit voltage was then collected using the NI USB-6008 data acquisition card and displayed on the computer via LabVIEW software. LabVIEW is a programming environment that utilizes graphical programming language for designing virtual instruments for experiments using the "G" language. The program designed in this article primarily uses the DAQ Assistant, which is the driver programming assistant of the NI acquisition card, to receive and process the collected data, which is then saved. During the experiment, the test subjects affixed the heart sound sensor onto the mitral valve auscultation area with medical tape and maintained a sitting posture for approximately 50 seconds while setting the sampling rate to 2000 Hz. The heart sound acquisition system built in the experiment collected the heart sound signal for 20 seconds. The acquired heart sound signal was then filtered and denoised by a 20Hz to 200Hz

bandpass filter and a 50Hz notch filter, respectively, after which the processed heart sound signal waveform was displayed on the front panel. The band-pass filter of the acquisition system is an 8th-order ellipse filter, while the notch filter is a 3rd-order Butterworth filter. The program also features the function of storing the collected heart sound signal and the function of playing the collected heart sound audio in real-time.

LabVIEW can enable mixed programming of graphical programming combined with the MATLAB language by using a MATLAB script node. In the LabVIEW program developed in this study, real-time heart sound data collected from the acquisition system is fed into a classification model trained in MATLAB. The program then predicts whether the heart sound is normal or abnormal based on the model, and displays the prediction results on the front panel.

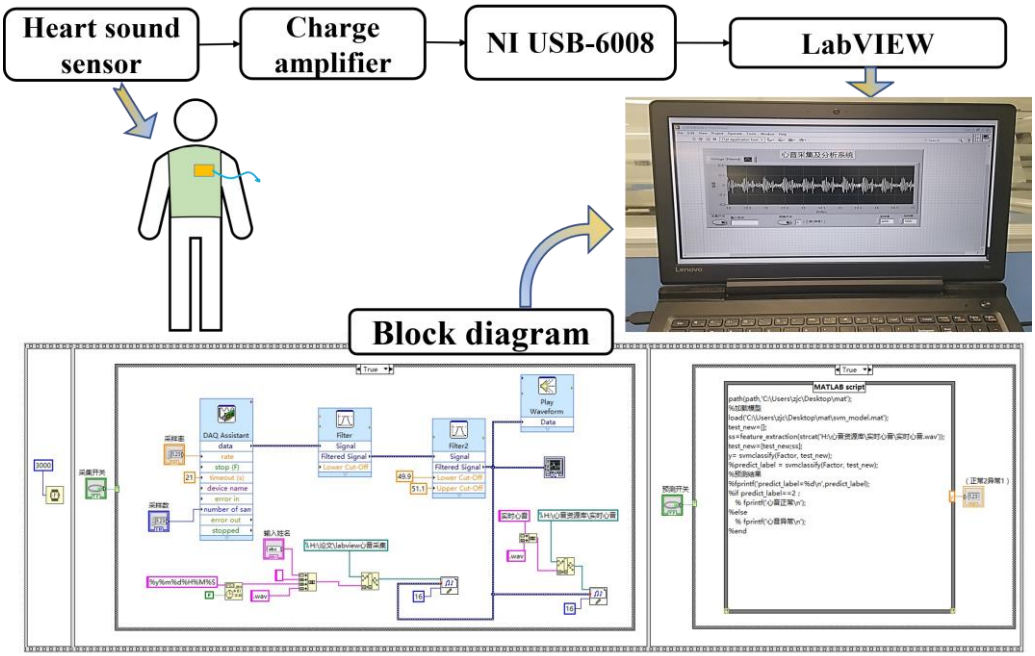

Figure 5: Block diagram of heart sound acquisition and classification system

By observing the waveform displayed on the front panel, it is evident that the signal filtered by the two filters exhibits distinct characteristics of the first and second heart sounds. When

observing the heart sound waveform, the collected heart sound can be heard by connecting headphones. The combination of audio and visual cues can more accurately differentiate normal or abnormal heart sound signals. Real-time collected heart sound signals are fed into the K-Nearest Neighbor (KNN) classification model for prediction. After waiting for approximately 5 seconds, the prediction result is displayed on the front panel as a numeric value: "1" indicates abnormal heart sound, while "2" indicates normal heart sound. In general, this heart sound acquisition system can quickly collect and predict heart sound signals, while also providing audio and visual output. The heart sound acquisition probe is soft, comfortable, and advanced, with the potential to become a new type of heart sound stethoscope.

Results and Discussion

Characterization of Thin Film Samples

In this paper, X-ray diffraction (XRD) was utilized to analyze the composition and β-phase content of composite piezoelectric nanofilms, while electron microscopy (SEM) was employed to observe the morphology of the thin film filaments. Figure 6 displays the XRD patterns of the three composite piezoelectric nanofilms. In the P(VDF-TrFE)/ZnO film, the mass fraction of ZnO is 10%, while in the P(VDF-TrFE)/ZnO/GR film, the mass fractions of ZnO and GR are 10% and 0.1%, respectively. The addition of ZnO resulted in the appearance of seven characteristic peaks, (100), (002), (101), (102), (110), (103), and (112) of ZnO on the XRD map of the composite nanofilm. This indicates that ZnO exists in the form of nanoparticles in the film fiber after being added to P(VDF-TrFE) [17-18].

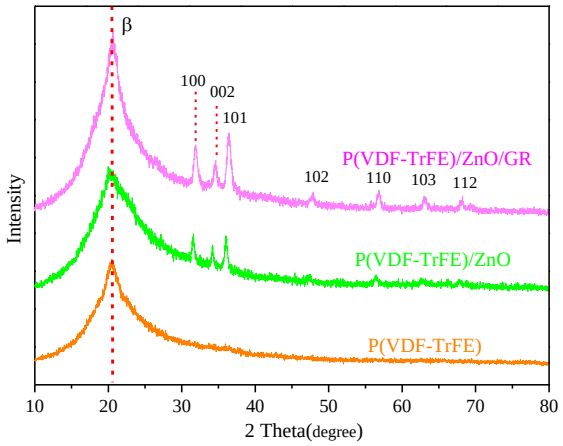

Figure 6: XRD patterns of three composite piezoelectric nanofilms

Upon comparison, it was observed that P(VDF-TrFE)/ZnO/GR films exhibited the highest β phase content among the three films, with P(VDF-TrFE)/ZnO showing slightly higher content than P(VDF-TrFE). Experimental results suggest that adding ZnO and trace amounts of GR filler can increase the β phase content of the composite piezoelectric film[19-21]. Higher β phase content is generally associated with better piezoelectric performance of the material.

The SEM images in Figure 7 reveal that the microstructure of nanofilms produced by electrospinning is composed of fibrous filaments at the micro-nano scale. SEM images of pure PVDF film in Figures 7(a) and 7(b) exhibit filamentous fibers with a relatively smooth surface. In contrast, Figures 7(c) and 7(d) show that the addition of ZnO to P(VDF-TrFE) composite nanofilm filaments leads to a rough and granular surface, caused by the aggregation of ZnO particles that embed onto the filament surface. By examining Figures 7(e) and 7(f), we observe that trace amounts of GR effectively inhibit the aggregation of ZnO particles, resulting in a smoother surface for P(VDF-TrFE)/ZnO/GR nanofilm filaments than P(VDF-TrFE)/ZnO.

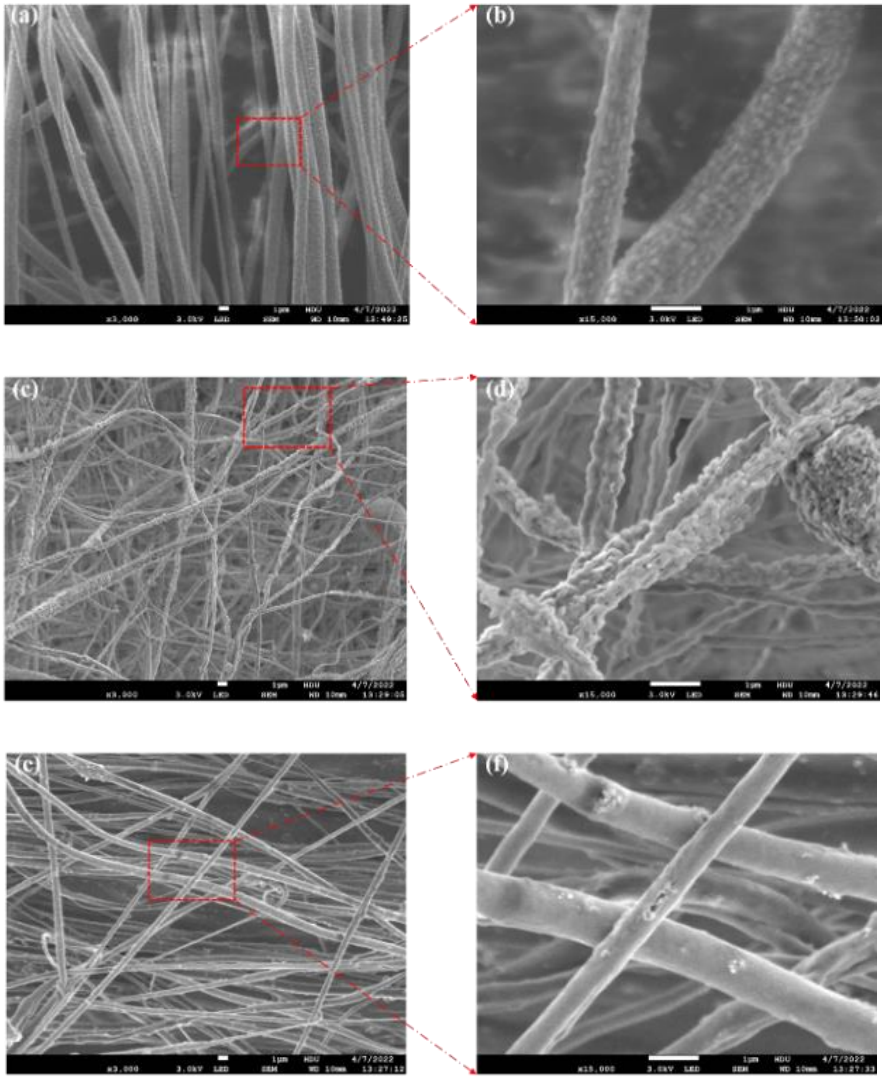

Figure 7: SEM diagram of P(VDF-TrFE) film (a), part of enlarged SEM diagram of Figure (b), SEM diagram of P(VDF-TrFE)/ZnO film (c), part of enlarged SEM diagram of Figure (d) and SEM diagram of P(VDF-TrFE)/ZnO/GR film(e), and enlarged SEM diagram of Figure (f).

Through calculation, as shown in Table 1, the average fiber diameters of P(VDF-TrFE), P(VDF-TrFE)/ZnO, P(VDF-TrFE)/ZnO/GR are 1.23μm, 0.78μm and 0.57μm, respectively. The addition of an appropriate amount of ZnO filler can improve the conductivity of the electrospinning solution, which leads to more thorough stretching of the fiber filaments under

the high-voltage electric field and a reduced filament diameter. Moreover, since GR has a sheet-like structure with good electrical conductivity, adding a trace amount of GR material can further enhance the solution's conductivity and promote the dispersion of ZnO particles, resulting in finer and smoother nanofiber filaments.

Table 1. Diameter of fibers for different filler films

The name of the material	P(VDF-TrFE)	P(VDF-TrFE)/ZnO	P(VDF-TrFE)/ZnO/GR
Diameter length/(μm)	1.23	0.78	0.57

Testing of Acoustic-electrical Conversion Performance

The heart sound signal consists of the first heart sound and the second heart sound, with a frequency range of 20 Hz to 200 Hz [22-23]. This signal is characterized by low sound pressure and medium to high frequency, and the heart sound sensor must exhibit good acoustic and electrical response frequency bandwidth in the range of 20 Hz to 200 Hz. To evaluate the sensor's acoustic-electrical conversion ability at the same frequency but varying sound pressure levels, we set the signal generator to emit a sine wave with a frequency of 180 Hz, and adjust the amplitude of the signal generator and power amplifier to control the sound pressure. We gradually increased the sound pressure from 65 dB to 85 dB, and measured the sensor response at 2 dB intervals, with the charge amplifier amplification set to 100 pC/V. To demonstrate that the P(VDF-TrFE)/ZnO/GR piezoelectric film has stronger acoustic-electrical conversion performance than the P(VDF-TrFE)/ZnO piezoelectric film and

the pure P(VDF-TrFE) piezoelectric film, we used these three films and the P(VDF-TrFE)/ZnO piezoelectric film with 10% ZnO and 0.1% GR as test samples. Figure 8 shows the results, with the response open-circuit voltage of the sensor gradually increasing with rising sound pressure, and the slope of the tangent line also increasing. At different sound pressures, the P(VDF-TrFE)/ZnO/GR sensors had higher response open-circuit voltage peaks than the P(VDF-TrFE) and P(VDF-TrFE)/ZnO sensors, indicating that the composite piezoelectric nanofilms with added ZnO and trace GR fillers showed stronger improvement in acoustic-electrical conversion performance. The acousto-electric conversion performance of the P(VDF-TrFE)/ZnO/GR sensors was greatly improved compared to the pure P(VDF-TrFE) and P(VDF-TrFE)/ZnO piezoelectric nanofilms, making it more suitable for sound energy collection.

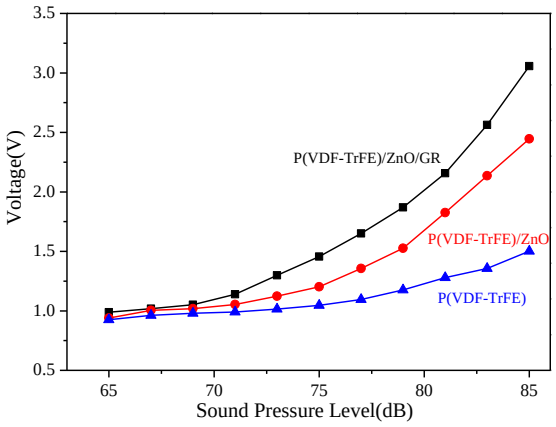

Figure 8: Voltage response diagram of the sensor at a sound frequency of 180 Hz and different sound pressure from 65 to 85 dB

The heart sound signal is characterized by low sound pressure and medium to high frequency components. A heart sound sensor should have good acoustic-electrical conversion capability in the frequency range of the heart sound signal. In this experiment, a signal

generator was used to produce a sine wave with a frequency range of 0 to 2000 Hz, with a frequency sweep step of 100 Hz/s. The sound pressure was set to 65 dB, and the charge amplifier's gain was set to 100 pC/V. Figure 9 shows the voltage traces recorded by the oscilloscope at different times during the frequency sweep. As seen in Figure 9, the peak open-circuit voltage significantly increases between frequencies of approximately 50 Hz to 200 Hz at a fixed 65 dB sound pressure.

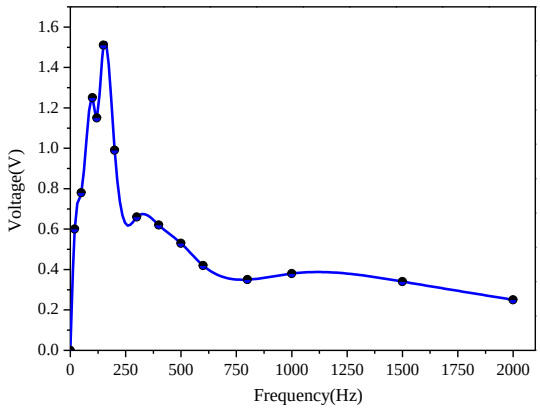

Figure 9: The sensor with 0 to 2 kHz swept-frequency voltage response at 65 dB sound pressure

To further verify the acoustic-electrical conversion performance of the sensor, the experiment measured its peak open-circuit voltage at 14 sound frequency points, as depicted in Figure 10, with a fixed sound pressure of 65 dB. The sensor developed in this study has a wide frequency response range, with excellent acoustic-electrical response performance in the frequency range of 20 Hz (the first test point) to 200 Hz (the sixth test point), satisfying the frequency response requirements of a heart sound sensor. Figure 11 illustrates the open-circuit voltage response of the sensor at different frequencies under a 65 dB sound pressure, showing a symmetrical voltage response about the 0 V line, with clear acoustic-electrical

response characteristics.

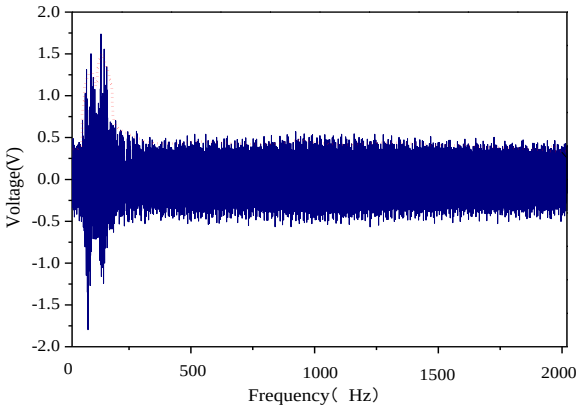

Figure 10: Different frequency voltage response diagram of the sensor at 65 dB sound pressure

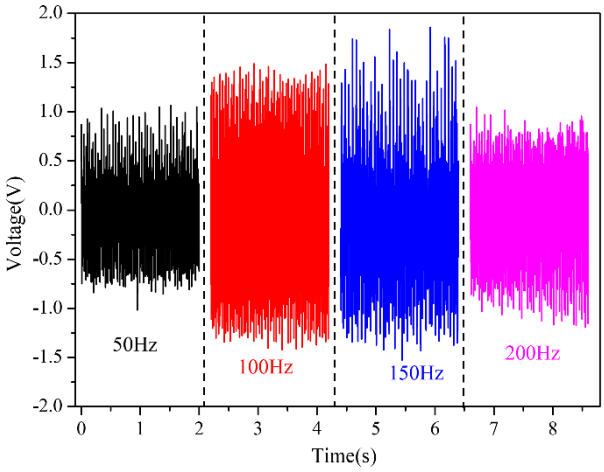

Figure 11: Open-circuit voltage plot of the sensor at 65 dB sound pressure at different frequencies

KNN Heart Sound Classification Recognition Algorithm

The K-Nearest Neighbor (KNN) classification algorithm is widely used in machine learning, and its fundamental classification idea is that a sample in a feature space belongs to the same category as the majority of its K nearest neighbors, and this sample has the same

characteristics as this class [24]. Since KNN mainly relies on the surrounding finite neighboring samples to determine the category characteristics, this method is more suitable for sample sets with more overlap or overlap of the class domain than other methods. The factors affecting the classification effect of KNN mainly lie in the selection of K value and the distance formula. For example, considering the two-dimensional heart sound data feature space shown in Figure 12, when K takes the constant value 3, and 2 of the 3 nearest samples to the sample being classified belong to class A, and 1 belongs to class B, so this sample belongs to category A, which means it is judged to be a normal heart sound. However, when K = 1, the sample being classified belongs to class B, meaning it is judged to be an abnormal heart sound. From this point of view, the selection of K value is the focus of constructing a KNN heart sound classification model. In this paper, the Euclidean distance calculation formula shown in the following equation is selected, and the most appropriate K value is determined by cross-validation.

$$d(x,y) = \sqrt{\sum_{i=1}^{n}(x_i - y_i)^2} \tag{1}$$

where d represents the distance. x_i and y_i represent the coordinates.

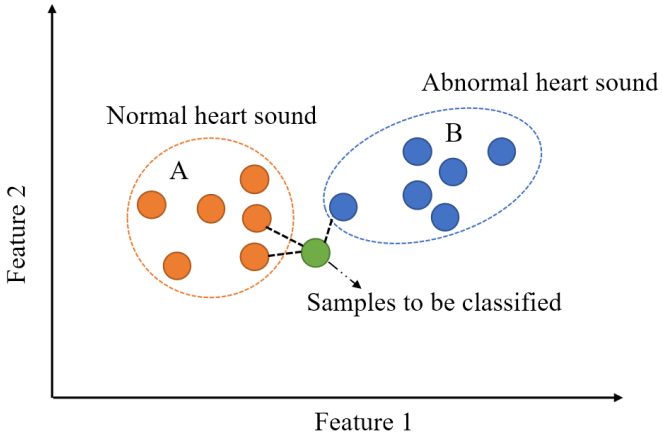

Figure 12: Example of KNN classification algorithm

The heart sound dataset chosen for the experiment consists of 65 sets of normal heart sound

data collected using homemade heart sound sensors and Physionet open-source data [25-26]. The 65 sets of heart sound data were collected from 13 adult human samples with normal heart sounds, and saved in WAV format using the experimental self-built heart sound acquisition system. The heart sound data in the PhysioNet/Computing in Cardiology Challenge 2016 (PhysioNet/CinC Challenge 2016) database includes 2461 normal heart sounds and 665 abnormal heart sounds in WAV format. All normal heart sounds are labeled -1 and all abnormal heart sounds are labeled 1. As the heart sound acquisition environment in the database is different, the collected heart sound signal may contain electromagnetic interference, lung sounds and other noise. In the experiment, a 20 to 200 Hz bandpass filter and 50 Hz notch filter were generated using MATLAB's built-in fdatool tool, both of which selected a third-order Butterworth filter. Since the amplitude of heart sound signals varies greatly due to the different devices used for collecting heart sound database data, the Z-Score function in MATLAB was employed to standardize the data signals separately, resulting in signal indicators in the same magnitude, increasing the comparability between data. Figure 13 shows a time domain diagram of a raw heart sound signal data (normal heart sound) in the heart sound database, while Figure 14 illustrates the time domain diagram of the preprocessed heart sound signal. Comparing the waveforms of the two figures, it can be observed that the characteristics of the first heart sound and the second heart sound of the preprocessed heart sound signal are more apparent, the noise removal effect is better, and the amplitude of the heart sound signal is improved. This is because the noise of the original heart sound signal is filtered out after passing through the filter, and the heart sound signal is characteristically scaled following the standardization operation.

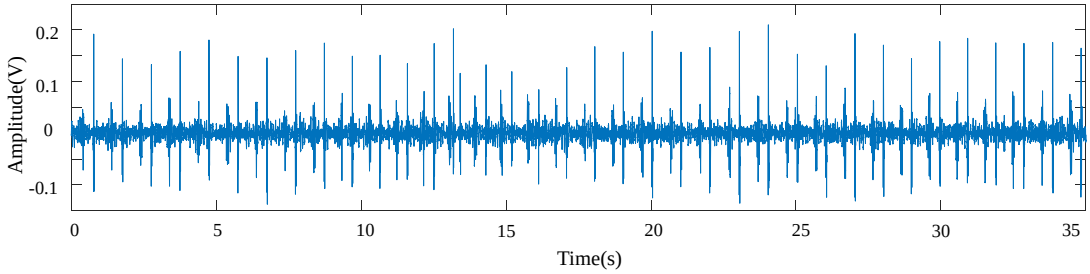

Figure 13: Heart sound time domain diagram before pretreatment

Fig.13 contains information from [PhysioNet/CinC Challenge 2016 database] which is made available under the Open Data Commons Attribution License v1.0, https://opendatacommons.org/licenses/by/1-0/.

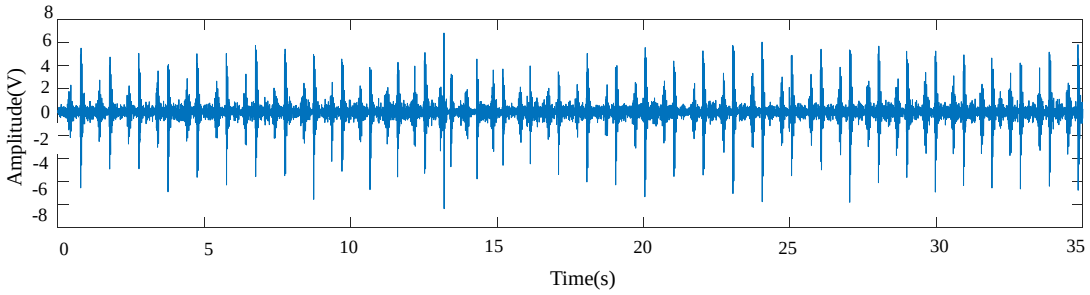

Figure 14: Heart sound time domain diagram after pretreatment

Fig.14 contains information from [PhysioNet/CinC Challenge 2016 database] which is made available under the Open Data Commons Attribution License v1.0, https://opendatacommons.org/licenses/by/1-0/.

In this experiment, 34 heart sound features were selected, including 14 time-domain features, 13 MFCC features, and 7 wavelet features. Table 2 displays the selected time and frequency domain features. MFCC is a speech feature that mimics the sensitivity of sound signals of different frequencies in the human ear, based on the hearing mechanism. Extracting MFCC features is useful for modeling heart sound signals. The wavelet feature extraction method

uses db6 wavelet decomposition to generate seven feature vectors. db6 wavelet decomposition decomposes the heart sound signal into five layers, selects seven optimal bases of the heart sound signal according to the filtering characteristics of the binary wavelet sub-band, reconstructed feature vectors. As shown in Figure 15, the shaded background annotation represents the 7 optimal bases that have been selected.

In this experiment, the Classification Learner toolbox in MATLAB was used to train a heart sound classification model. This toolbox allowed us to explore supervised machine learning by selecting various classifiers, exploring data, selecting features, specifying validation scenarios, training models, and evaluating results. Automated training was used to search for the best classification model types, including decision trees, support vector machines, logistic regression, and KNN. After cross-validation, fine KNN (with a K value of 1) was chosen as the heart sound classification model.

Table 2. Selected 14 heart sound signatures in the time and frequency domains

Number	Feature name
1	Mean value characteristics of heart sound signal data
2	Median characteristics of heart sound signal data
3	Standard deviation characteristics of heart sound signal data
4	Characteristics of mean absolute deviation of heart sound signal data
5	Quantile characteristics of heart sound signal data (25%)
6	Quantile characteristics of heart sound signal data (75%)
7	4th percentile difference of heart sound signal data
8	Deviation of heart sound signal data
9	Kurtosis of heart sound signal data
10	Shannon entropy of heart sound signal data

11	Spectral entropy of heart sound signal data
12	Frequency characteristics of heart sound signal data: dominant frequency, dominant frequency ratio, dominant frequency amplitude
13	
14	

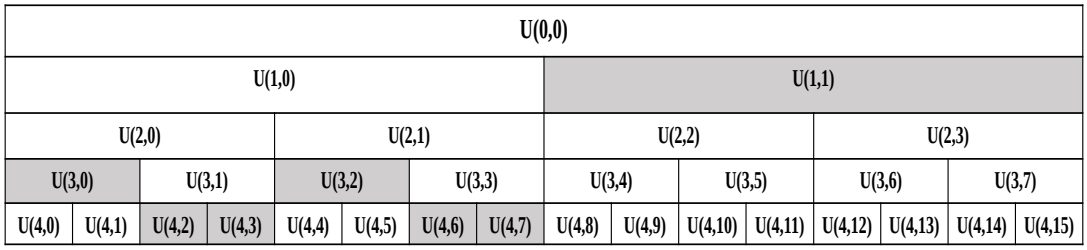

Figure 15: Wavelet packet decomposition and optimal basis selection diagram

The verification method used is cross-validation. The heart sound data is divided into 5 equal copies, where 4 copies are utilized for model training and 1 copy is used for validation. The training and validation are alternately rotated for 5 times, and the average of the 5 validation results is computed to measure the accuracy of the model. The recognition rate is adopted as the metric to assess the quality of the classification model, and was calculated using equation (2) as stated below:

$$Accuracy = \frac{TP+TN}{TP+TN+FP+FN} \quad (2)$$

The term *"TP"* represents the number of heart sounds that were correctly identified as normal, while *"FN"* represents the number of normal heart sounds that were mistakenly classified as abnormal. *"TN"* represents the number of heart sounds with ..abnormal sounds that were correctly identified as such, and *"FP"* represents the number of abnormal heart sounds that were mistakenly classified as normal. After verification, the heart sound classification model trained in the experiment achieved an accuracy rate of 94.8%.

According to Liu et al. [27] in 2022, adaptive noise-complete empirical modal decomposition

permutation entropy combined with a support vector machine was used to classify normal and abnormal heart sound samples in the PhysioNet/CinC Challenge 2016 database, and the classification accuracy was 87%. In comparison, the KNN heart sound classification model has better accuracy for normal and abnormal classification of heart sound signals than the support vector machine classifier proposed by Liu et al. The confusion matrix of the heart sound classification model is shown in Figure 16. The matrix indicates that this classification model has an 11.1% probability of misclassifying abnormal heart sound signals as normal heart sounds, and a 3.3% probability of misclassifying normal heart sound signals as abnormal heart sounds. This might be due to the fact that there are more normal heart sounds than abnormal heart sounds in the heart sound signal data. Therefore, further supplementation of heart sound data is needed to optimize the heart sound classification model.

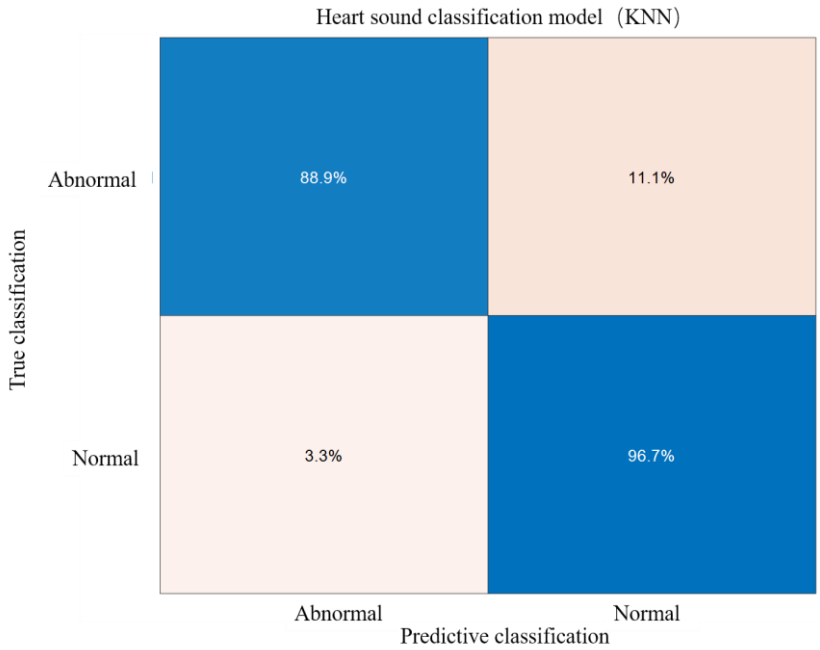

Figure 16: Validation confusion matrix of heart sound classification model (fine KNN).

Figure 16 displays the validation confusion matrix of the heart sound classification model (fine KNN). The model trained in this paper can accurately predict normal and abnormal heart sounds. When combined with the heart sound acquisition system built in the previous section, it can fulfill the entire process from heart sound collection to heart sound diagnosis, thereby providing a new solution for the study of heart disease.

Conclusion

In this paper, P(VDF-TrFE)/ZnO/GR flexible piezoelectric composite films with excellent acoustic-electrical conversion performance were prepared using the electrospinning process. Electron microscopy revealed that the filaments of P(VDF-TrFE)/ZnO/GR films had finer and smoother characteristics than those of P(VDF-TrFE)/ZnO flexible piezoelectric composite films without GR. Analysis of X-ray diffraction patterns indicated that the β phase content of P(VDF-TrFE)/ZnO/GR piezoelectric composite films was higher than that of P(VDF-TrFE)/ZnO and P(VDF-TrFE). P(VDF-TrFE)/ZnO/GR was packaged into a flexible piezoelectric nano heart sensor, and the outermost layer of silica gel effectively protected the flexible nano film and adhered to the skin. In this paper, the acoustic-electrical conversion performance of P(VDF-TrFE)/ZnO/GR piezoelectric composite films was evaluated using a self-built acoustic-electrical conversion performance test platform. Experimental comparisons revealed that the P(VDF-TrFE)/ZnO/GR piezoelectric composite films exhibited superior acoustic-electrical conversion performance in comparison to P(VDF-TrFE) piezoelectric films. Frequency sweeping experiments revealed that the experimentally prepared P(VDF-TrFE)/ZnO/GR piezoelectric composite nanofilms exhibited excellent acoustic-electrical

conversion performance under low-frequency and medium-frequency sound signals, meeting the requirements for good acoustic-electrical conversion ability in the frequency range of heart sound signals.

In this paper, the KNN heart sound classification model was trained using MATLAB. Additionally, a heart sound acquisition platform was constructed using LabVIEW, which calls the MATLAB script to input real-time heart sound signals into the trained heart sound classification model for predicting normal and abnormal heart sounds.

The wearable flexible nano-heart sound sensor made of P(VDF-TrFE) designed in this paper, combined with the self-built heart sound acquisition system, is capable of predicting the normality of real-time heart sound signals. In comparison to traditional heart sound stethoscopes, this sensor offers the advantages of being soft and close to the skin, while the use of a machine learning algorithm to classify heart sound signals normality solves the shortcomings of traditional auscultation, such as introducing murmurs and relying on personal experience for interpretation.

Acknowledgements

The experimental procedures involving human subjects in the manuscript strictly adhered to the ethical principles outlined in the 1964 Helsinki Declaration (revised in 2013). Each participant was informed and gave their consent to be included in the study prior to their involvement. The authors sincerely appreciate the participation of every individual involved in this research presented in the manuscript.

ORCID® iDs

Yi Luo - https://orcid.org/0000-0002-1528-788X

Jian Liu - https://orcid.org/0009-0007-6816-3948

Jiachang Zhang - https://orcid.org/0000-0002-6636-0135

Yu Xiao - https://orcid.org/0009-0007-7909-6410

Ying Wu - https://orcid.org/0009-0003-2722-731X

Zhidong Zhao - https://orcid.org/0009-0008-7945-8466

References

1. World health statistics 2021: monitoring health for the SDGs, sustainable development goals. Geneva: World Health Organization.
2. Santiago I F, Blanca T, René L. Deep Learning Algorithm for Heart Valve Diseases Assisted Diagnosis[J]. Applied Sciences,2022,12(8):3780
3. Markel, Howard. The Stethoscope and The Art of Listening[J]. The New England Journal of Medicine, 2006, 354(6): 551-553
4. Electronic Stethoscope Filtering Mimics the Perceived Sound Characteristics of Acoustic Stethoscope[J]. IEEE journal of biomedical and health informatics,2020, PP.
5. Felipe S, José S, Veronica I, et al. Electronic stethoscope – a didactic and low cost acquisition system for auscultation[J]. International Journal of Biosensors & Bioelectronics, 2019,5(5).

6. Yogeswaran V, Kanade R, Mejia C, et al. Role of Doppler echocardiography for as sessing right ventricular cardiac output in patients with atrial septal de-fect[J]. Conge nital heart disease, 2019,14(5):713-719.
7. Agarwal R, Gosain P, Kirkpatrick J N, et al. Tissue Doppler imaging for diag-nosis o f coronary artery disease: a sy-stematic review and meta-analysis[J]. Cardiovascular Ultrasound, 2012, 10-(1):47.
8. Sumber, Setioningsih E, Hamzah T. Comparison of Bluetooth Performance f-or Low-Cost Wireless Stethoscope Implementation in Terms of Data Loss[J].Journal of Biom imetics, Biomaterials and Biomedical Engineering,2022,6300:288-299.
9. Liu B, Han, Pan L, et al. Flexible Mul-tiscale Pore Hybrid Self-Powered Sen-sor for Heart Sound Detection[J]. Sen-sors (Basel, Switzerland),2021,21(13):-4508.
10. Y, Tajitsu. Piezoelectric Properties of Ferroelectrics[J]. Ferroelectrics 2011, 415:57–66.
11. Liu M, Liu Y, Zhou L. Novel Flexible PVDF-TrFE and PVDF-TrFE/ZnO Pre-ssure S ensor: Fabrication, Characteriz-ation and Investigation[J]. Micromachi-nes, 2021, 12 (6):602.
12. Pi Z, Zhang J, Wen C, et al. Flexible piezoelectric nanogenerator made of poly(vin ylidenefluoride-co-trifluoroethyl-ene) (PVDF-TrFE) thin film[J]. Nano Energy,2014,7:3 3-41.
13. Kumar M, Kumari P, Sahatiya P. P(V-DF-TrFE)/ZnO nanofiber composite ba-sed pie zoelectric nanogenerator as se-lfpowered sensor: fabrication and cha-racterization[J]. Journal of Polymer R-esearch, 2022, 29(2):1-16.

14. Subash C K, Sreenidhi P R, Varghese S. Poly(vinylidene fluoride-trifluoroeth-ylene)-ZnO Nanoparticle Composites on a Flexible Polydimethylsiloxane Su-bstrate for Energy Harvesting[J].Acs Applied Nano Materials, 2019，2(7)： 4350-4357.
15. Zheng Y, Guo X, Qin J, et al. Compu-ter-assisted diagnosis for chronic heart failure by the analysis of their cardiac reserve and heart sound characterist-ics[J]. Computer Methods Programs B-iomed,2015,122 (3): 372-383.
16. Huang C, Thomas N L. Fabrication of porous fibers via electrospinning: strat-egies and applications[J]. Polymer Re-views,2019,60(4):1-53.
17. Rlk A, Psvn B, Ppnvk C, et al. Antibi-otic potentiation and anti-cancer comp-etence through bio-mediated ZnO nan-oparticles[J]. Materials Science & Eng-ineering C,2019,103(C):109756.
18. Athauda T J, Neff J G, Sutherlin L, et al. Systematic study of the structure propert y relationships of branched hie-rarchical TiO2/ZnO nanostructures[J]. Acs Appl Mater Interfaces, 2012, 4(1-2):6917-6926.
19. Zhu G, Yang R, Wang S, et al. Flexi-ble high-output nanogenerator based on lateral ZnO nanowire array [J]. Na-no Lett, 2010, 10(8): 3151-3155.
20. Shi L, Jin H, Dong S, et al. High-perf-ormance triboelectric nanogenerator b-ased on electrospun PVDF-graphene nanosheet composite nanofibers for e-nergy harvesting[J]. Nano Energy,2021,80.
21. Dodds J S. Meyers F N, Loh K J. Pi-ezoelectric Characterization of PVDF- TrFE Thin Films Enhanced With ZnO Nanoparticles[J]. IEEE Sensors Journ-al, 2012, 12(6):1889-1890.

22. Liu C, Springer D, Li Q, et al. An op-en access database for the evaluation of hear t sound algorithms[J]. Physiol-ogical Measurement, 2016, 37(12):21-81-2213.
23. Debbal S M, Bereksi-Reguig F. Comp-uterized heart sounds analysis[J]. Per-gamon Press, Inc. 2008, 38(2):263-28-0.
24. Patrick E A, Iii F. A generalized k-nea-rest neighbor rule[J]. Information & C-ontrol, 1970, 16(2):128-152.
25. Liu C, Springer D, Li Q, Moody B, Juan RA, Chorro FJ, Castells F, Roig JM, Silva I, Johnson AE, Syed Z, Schmidt SE, Papadaniil CD, Hadjileontiadis L, Naseri H, Mo ukadem A, Dieterlen A, Brandt C, Tang H, Samieinasab M, Samieinasab MR, Same ni R, Mark RG, Clifford GD. An open access database for the evaluation of heart s ound algorithms. Physiol Meas.2016 Dec;37(12):2181-2213. https://iopscience.iop.org/ article/10.1088/0967-3334/37/12/2181. DOI: 10.1088/0967-3334/37/12/2181.
26. Goldberger, A.; Amaral, L.; Glass, L.; Hausdorff, J.; Ivanov, P.C.; Mark, R.; Mietus, J.E.; Moody, G.B.; Peng, C.K.; Stanley, H.E. PhysioBank, PhysioToolkit, and Physio Net: Components of a new research resource for complex physiologic signals. Circu lation 2000, 101 (23), e215–e220. doi:10.1161/01. CIR. 101.23.e215
27. Liu M, Wu Q, Ding S. A heart sound classification method based on compl-ete ens emble empirical modal decom-position with adaptive noise permutati-on entropy and support vector machi-ne [J]. Journal of Biomedical Engineering,2022,39(02):311-319.